JOURNAL OF Materials CHEMISTRY

Chemical, structural and electrical characterizations in the BIZNVOX family

Christine Vernochet,[a] Rose-Noëlle Vannier,[a] Marielle Huvé,[a] Caroline Pirovano,[a] Guy Nowogrocki,*[a] Gaëtan Mairesse*[a] and Gustaaf Van Tendeloo[b]

[a]*Laboratoire de Cristallochimie et Physicochimie du Solide, ESA CNRS 8012, Ecole Nationale Supérieure de Chimie de Lille, BP 108, 59652 Villeneuve d'Ascq Cedex, France mairesse@ensc-lille.fr*
[b]*EMAT, University of Antwerp (RUCA), Groenenborgerlaan 171, B-2020 Antwerp, Belgium*

Received 31st July 2000, Accepted 11th September 2000
First published as an Advance Article on the web 27th October 2000

The BIZNVOX solid solution domain, stable at room temperature, has been determined. α-, β- and γ-type compounds can be stabilized depending on the x and y values of the general $Bi_2(V_{1-x-y}Zn_xBi_y)O_z$ formula. The α- and β-type phases exhibit incommensurate modulations studied by X-ray powder diffraction. The lock-in of their wave vectors on the three-fold and two-fold superstructures of the undoped α- and β-$Bi_4V_2O_{11}$, respectively, is clearly evidenced. SAEDand HREM observations reveal very complex disorder correlated with the attractive oxide ion conductivity of these materials.

Introduction

The two-dimensional fast oxide ion conducting BIMEVOX's display very attractive electrical properties at moderate temperature and are currently under intensive study to optimise their performance.[1–4] The parent compound of this family, $Bi_4V_2O_{11}$, contains intrinsic oxygen vacancies and exhibits three crystallographic polymorphs α, β and γ with transition temperatures α↔β and β↔γ at about 400 and 600 °C, respectively. Long range vacancy ordering is responsible for these phase transitions, but substitution of isovalent or aliovalent cations ME for V can suppress the transitions and stabilise the β- or the γ-type phases to room temperature.[5–7]

A large variety of ME dopants have already been investigated but most of these previous studies have focussed on the single ME→V substitution, whereas in fact the BIMEVOX solid solutions have to be delimited in a Bi_2O_3–V_2O_5–ME_xO_z ternary diagram. We report here a detailed study of the structural and electrical properties of Zn doped phases and their compositional dependence. The Zn^{2+} cation has a special electronic configuration $3d^{10}$ leading to only one valence state to consider, and the absence of crystal field stabilisation enables it to accommodate various coordinations with oxygen: mainly tetrahedral but also octahedral and trigonal bipyramidal.

Some electrical and structural data and their correlation with the conduction properties limited to the BIZNVOX.10 composition *i.e.* $Bi_2V_{0.9}Zn_{0.1}O_z$ have already been reported.[8–10] But the first presentation of the corresponding BIZNVOX solid solution area was published by Lee *et al.* and several mechanisms, including the possible partial occupancy of Bi sites by Zn together with the creation of interstitial Zn^{2+} cations, were proposed.[11] For reasons largely explained in our study of the BICOVOX solid solution,[12] we believed that the single phase domain was greatly overestimated by these authors and we proposed a more limited one corresponding to the $Bi_2V_{1-x-y}Zn_xBi_yO_z$ formula, with only positive values for both x and y.[13]

More recently, Krok *et al.* published a study on electrical conductivity and structure correlation in BIZNVOX investigated by X-ray powder diffraction and ac impedance spectroscopy, but this study was limited to the $Bi_2V_{1-x}Zn_xO_z$ join.[14]

This paper completes our preliminary brief report and in the first part we tentatively describe the different steps of the BIMEVOX synthesis by the classical solid-state method and the appropriate precautions necessary to obtain pure phases. The second part is devoted to the presentation of the compositional extent of the α-, β- and γ-type domains of the BIZNVOX solid solution stable at room temperature. A particular emphasis is placed upon the incommensurate compositional modulations observed by X-ray powder diffraction and selected area electron diffraction (SAED) and their correlation with the conduction properties.

Experimental

The synthesis of powdered BIZNVOX was performed by the classical solid-state method, starting from stoichiometric amounts of reagent grade Bi_2O_3 (99.9%, Aldrich, previously decarbonated at 600 °C for 6 h), V_2O_5 (99.6%, Aldrich) and ZnO (99.9%, Cerac). The weighed oxides were mixed and ground in an agate mortar, and then fired in Au foil boats for 12 h successively at 600, 700 and 800 °C with intermediate regrinding.

Samples were analysed by X-ray powder diffraction (at room temperature: Guinier-De Wolf focusing camera, Cu-Kα radiation; at high temperature: Guinier-Lenné camera, scan rate 0.3 °C min^{-1}). Unit cell parameter refinements were performed with data collected using a Siemens D5000 goniometer (Cu-Kα radiation, graphite monochromator). High temperature X-ray diffraction (HTXRD) diagrams under a controlled atmosphere were obtained with the same diffractometer, using a HTK 1200 Anton Paar device and a PSD detector, the sample was deposited on a thin gold foil on the alumina holder. A diagram was recorded every 15 min in the 10–70° 2θ domain, with a 5 min delay before each measurement, a step of 0.0146° and a counting time of 0.15 s (*i.e.* a diagram was recorded in about 10 minutes).

DTA analysis was made using a Setaram 92 thermal analysis system with a platinum crucible up to 900 °C (scan rate

5 °C min^{-1}). DSC measurements were made using a Du Pont Instrument 910 with a gold crucible up to 600 °C (scan rate 10 °C min^{-1}).

Ionic conductivity measurements were performed in air during heating and cooling, with an SI 1255 frequency range analyser (Schlumberger) in the frequency range 1–10^6 Hz. Two heating–cooling cycles were carried out between 200 and 800 °C in steps of 20 °C, with 1 h stabilisation prior to impedance measurement.

Density measurements were carried out using a Micromeritics Accupyc 1330 helium pycnometer, with a 1 ml sample capacity.

High resolution images and electron diffraction patterns were obtained on a JEOL 4000EX with point resolution of 1.7 Å, and JEOL 200CX. The material was crushed and dispersed on a holey carbon film deposited on a Cu grid. The computer simulated HREM images were calculated using the Mac Tempas program.

Results and discussion

Mechanism of BIMEVOX synthesis

We have already mentioned some difficulties associated with the preparation of pure $Bi_4V_2O_{11}$ and derived BIMEVOX compounds by the classical solid-state method, leading to $BiVO_4$ and/or $Bi_8V_2O_{17}$ as impurities.[15] To establish the mechanism of BIMEVOX formation, a DTA and a high temperature X-ray powder diffraction study were performed on a crude mixture of $1Bi_2O_3$–$0.4V_2O_5$–0.2ZnO corresponding to the BIZNVOX.20 composition. The DTA and HTXRD patterns are reported on Figs. 1 and 2, respectively.

The DTA curve is particularly complex and can be characterized by: (1) a departure from linearity occurring around 380 °C, (2) a series of exothermic effects between 550 and 650 °C followed by another series of endothermic effects between 720 and 790 °C and (3) a significant endothermic peak at about 870 °C corresponding to BIZNVOX melting.

The Guinier-Lenné diffraction pattern displays, at first sight, three main modifications around 400, 500 and 750 °C, respectively (Fig. 2). At about 400 °C, the diffraction lines of $BiVO_4$ already appear. The formation of this compound is very easy and seems to be associated with the first endothermic effect starting around 380 °C on the DTA curve. Around 500–550 °C, two steps can be identified: appearance of γ-Bi_2O_3 and $Bi_8V_2O_{17}$ like-phases, followed by the decreasing intensity of the lines assigned to γ-Bi_2O_3 and V_2O_5 concomitant with the appearance of the BIZNVOX compound. Finally, around 750 °C two new steps are noticed: the disappearance of γ-Bi_2O_3 followed by that of $BiVO_4$.

As a matter of fact, the experimental conditions of DTA and HTXRD involve very different heating rates. Moreover, the Guinier-Lenné sample is a largely dispersed powder mixture on a gold grid and consequently there is a poor quality contact between the starting reagents leading to some $Bi_8V_2O_{17}$ remaining in addition to the expected BIZNVOX.

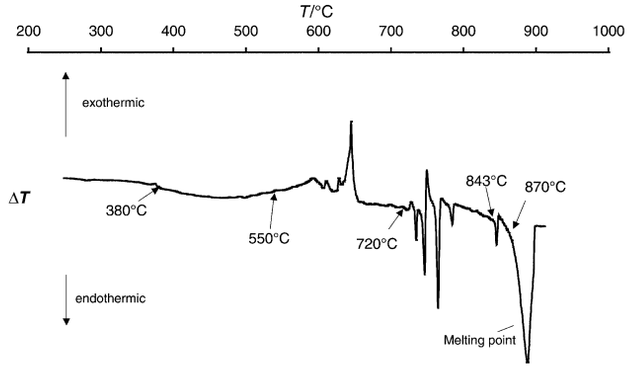

Fig. 1 DTA performed on a crude mixture of $1Bi_2O_3$–$0.4V_2O_5$–0.2ZnO corresponding to the BIZNVOX.20 composition.

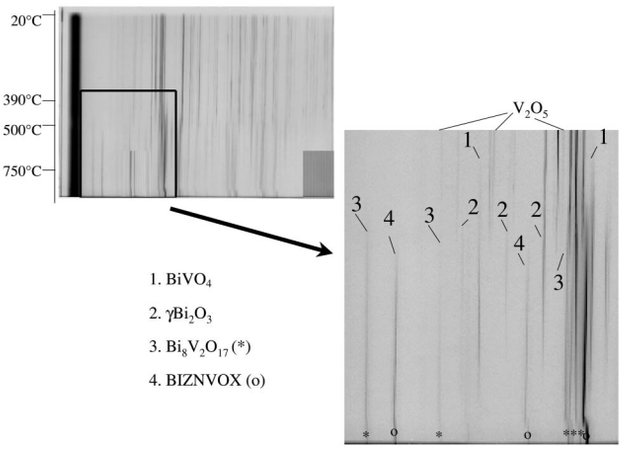

Fig. 2 HTXRD performed with a Guinier-Lenné camera on a crude mixture of $1Bi_2O_3$–$0.4V_2O_5$–0.2ZnO corresponding to the BIZNVOX.20 composition.

These *in situ* dynamic characterizations were pursued by static experiments: the same mixture of crude powder corresponding to the same starting composition was heated successively at 600, 700 and 800 °C for 15 h. Between two consecutive heating treatments, the powder was quenched in air, reground and analysed by X-ray diffraction at ambient temperature. The X-ray patterns are reported on Fig. 3 and can be ascribed as follows:

After 15 h at 600 °C, a temperature below the V_2O_5 melting point (690 °C), a mixture of γ-Bi_2O_3, δ-Bi_2O_3, V_2O_5, $Bi_8V_2O_{17}$, $BiVO_4$ and BIZNVOX is clearly observed.

After a further 15 h at 700 °C, the amount of BIZNVOX has obviously increased, whereas $BiVO_4$ and $Bi_8V_2O_{17}$ are the only remaining crystallised phases.

After the last 15 h treatment at 800 °C, pure BIZNVOX.20 is obtained.

All these dynamic and static observations are coherent. The small difference observed in the static experiment is the presence of δ-Bi_2O_3, not identified by HTXRD, which is due to the partial transformation of some of the γ-Bi_2O_3 into δ-Bi_2O_3 during the quenching of the sample to room temperature. Thereby, the mechanism of formation seems to be characterized by the intermediate synthesis of both $BiVO_4$ and $Bi_8V_2O_{17}$ compounds, which then react with each other to form the pure expected phase.

Very similar general observations were made when preparing other BIMEVOX materials or/and $Bi_4V_2O_{11}$, and therefore the

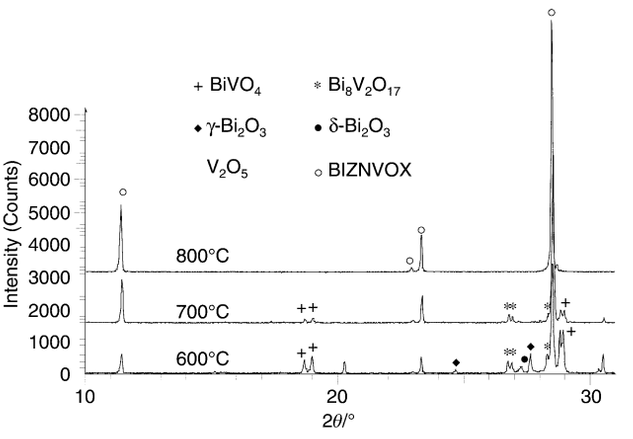

Fig. 3 XRD patterns corresponding to a mixture of $1Bi_2O_3$–$0.4V_2O_5$–0.2ZnO successively treated at 600, 700 and 800 °C.

simplified general mechanism of synthesis, neglecting the ME dopant, can be described as: (1) formation of $BiVO_4$: $2(Bi_2O_3+V_2O_5\rightarrow 2BiVO_4)$; (2) formation of $Bi_8V_2O_{17}$: $4Bi_2O_3+V_2O_5\rightarrow Bi_8V_2O_{17}$; (3) reaction between these intermediate compounds according to $4BiVO_4+Bi_8V_2O_{17}\rightarrow 3Bi_4V_2O_{11}$.

The global reaction (1)+(2)+(3) leads to $6Bi_2O_3+3V_2O_5\rightarrow 3Bi_4V_2O_{11}$ and is in accordance with the stoichiometry of the synthesis of $Bi_4V_2O_{11}$ from a 2/1 molar ratio of Bi_2O_3 and V_2O_5. This basic mechanism accounts for some of the problems frequently observed when trying to prepare directly $Bi_4V_2O_{11}$ or BIMEVOX in a one-step process at high temperature, leading to some unreacted $BiVO_4$ and/or $Bi_8V_2O_{17}$-type impurities.

BIZNVOX

The loci of the solid solution were established using classical X-ray powder diffraction. For some specific compositions, density measurements were performed for comparison with theoretical values. The solid solution domain is reported in Fig. 4 and is in fair agreement with our preliminary report. The dotted line corresponds to the domain as proposed by Lee *et al.*[11] determined from air quenched materials. Both domains are fairly similar along the stoichiometric join $Bi_2V_{1-x}Zn_x$ ($y=0$), but from our study no extent towards V_2O_5 is observed since for such starting compositions ZnO is systematically detected as an impurity. In the same way, for y values larger than 0.05, towards the Bi rich part of the diagram, a $Bi_8V_2O_{17}$-type impurity is revealed.

To ascertain the mechanism responsible for the extent of the solid solution when $y>0$ (Bi excess), density measurements were performed on three global compositions with a fixed amount of Zn and increasing amounts of Bi: $Bi_2V_{0.80}Zn_{0.20}O_z$ (A); $Bi_2V_{0.765}Zn_{0.2}Bi_{0.035}O_z$ (B) and $Bi_2V_{0.75}Zn_{0.2}Bi_{0.05}O_z$ (C). The results are reported in Table 1 and compared with the calculated values corresponding to different hypotheses. As in the case of BICOVOX, the experimental values unequivocally agree with the mechanism according to which V is substituted by the excess of Bi.

Comparing our results with those of Krok *et al.*[14] along the stoichiometric join $Bi_2V_{1-x}Zn_x$ (without excess Bi, $y=0$), the upper limit of the solid solution is very similar: $x=0.25$ (our results), compared to $x=0.27$, this difference being within the experimental uncertainty. Some question was raised by Krok *et al.* about the existence of a β domain between 0.075 and 0.125 as we proposed. This domain is clearly evidenced on the X-ray diffraction patterns reported in Fig. 5. Indeed, from a structural point of view, the three polymorphs of $Bi_4V_2O_{11}$ can be described from an orthorhombic "mean cell" with lattice parameters $a_m\approx 5.53$, $b_m\approx 5.61$ and $c_m\approx 15.29$ Å at 20 °C.[15] The high temperature γ-polymorph is tetragonal with

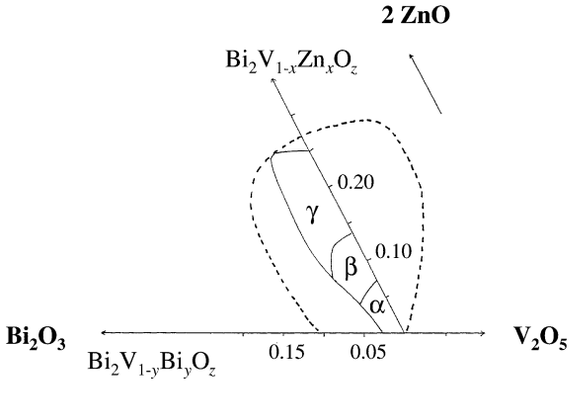

Fig. 4 BIZNVOX solid solution domain compared to that found by Lee *et al.*[11] (in dotted line) obtained on air quenched materials.

Table 1 Comparison of experimental and theoretical densities calculated from three hypotheses: Bi in V sites (1), V vacancies (2) and "interstitial sites" (3)

Compound	d_{exp}	d_1	d_2	d_3
$Bi_2V_{0.80}Zn_{0.20}O_z$ (A)	7.70(3)	7.66	7.66	7.66
$Bi_2V_{0.765}Zn_{0.20}Bi_{0.035}O_z$ (B)	7.73(3)	7.71	7.58	7.99
$Bi_2V_{0.75}Zn_{0.20}Bi_{0.05}O_z$(C)	7.76(3)	7.73	7.54	8.13

$a_t=b_t=a_m/\sqrt{2}$. The β-polymorph is characterised by a two-fold superstructure with a doubling of the a_m axis, orthorhombic unit cell, while the room temperature α-polymorph reveals a six-fold superstructure along the a_m axis combined with a small monoclinic distortion but by X-ray powder diffraction a three-fold superstructure with $a=3a_m$ is practically only observed.

When substituting Zn for V, the X-ray diffraction patterns are characterized by an α-type structure up to $x=0.075$. More precisely, when $x=0.025$ the monoclinic supercell is modified to an orthorhombic one with the same apparent superstructure $=3a_m$, which is a classical behaviour observed practically whatever the nature of the ME dopant. The $x=0.10$ and $x=0.125$ compositions exhibit the typical pattern of a β-type cell, and then for larger x values a γ-type quadratic cell is obtained.

The X-ray diffractograms corresponding to these different compositions are reported on Fig. 5 and the variation of the a_m and b_m parameters is shown on Fig. 6. The β-type domain does really exist. Moreover, the intensity of the satellite peaks is high enough in this BIZNVOX family to undertake their indexation, but this indexation requires the use of a four-dimensional reciprocal lattice vector written $\boldsymbol{G}=h\boldsymbol{a}_m^*+k\boldsymbol{b}_m^*+l\boldsymbol{c}_m^*+m\boldsymbol{q}=\boldsymbol{H}+m\boldsymbol{q}$ where $\boldsymbol{q}=\delta\boldsymbol{a}_m^*$ is the modulation vector and $\boldsymbol{H}$ is any

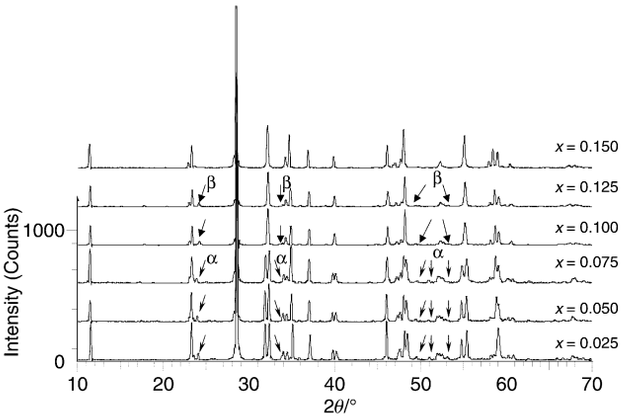

Fig. 5 Diffraction patterns corresponding to $Bi_2V_{1-x}Zn_xO_z$ compositions (arrows indicate α and β modulations respectively).

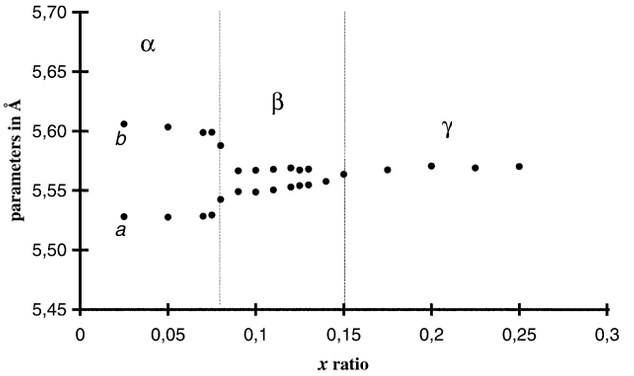

Fig. 6 $Bi_2V_{1-x}Zn_xO_z$ unit cell parameters refined in the "mean cell".

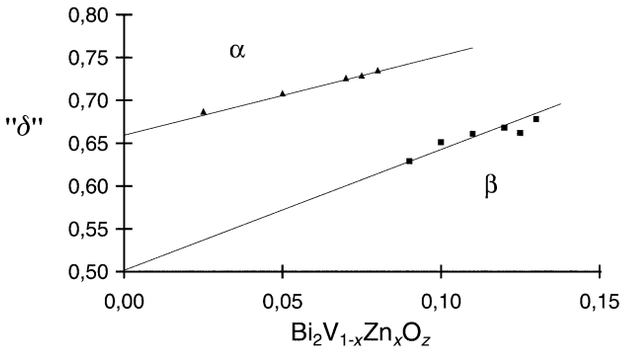

Fig. 7 Modulation coefficient δ *versus* x substitution ratio corresponding to $Bi_2V_{1-x}Zn_xO_z$.

basic reciprocal lattice vector. The variation of δ *versus* x is drawn on Fig. 7. A smooth proportional variation of δ with x is observed, characterising an incommensurate compositional modulation. In fact, two variation rates are observed in the α- and β-type domains, respectively, with a discontinuity around $x=0.08$ which confirms the compositional limit of the α⟶β transformation. Furthermore, extrapolation of the two straight lines to $x=0$ leads to δ values = 0.66 and 0.50 for α and β, respectively, which correspond to the $3a_m$ and $2a_m$ superstructures in direct space. This lock-in of the incommensurate modulations on the commensurate superstructures of the undoped parent compound $Bi_4V_2O_{11}$ is a classical characteristic of the compositional incommensurate modulations. Similar observations on other BIMEVOX have already been described in BIMOVOX[16] and BIWVOX,[17] but were limited to β-type structures.

The DSC curves (Fig. 8) are in agreement with these structural observations. For $x=0.025$ the typical α↔β and β↔γ reversible phase transitions are observed, with a noticeable hysteresis of the β⟶α transition during the cooling process. For $x=0.05$ the two transitions coalesce with each other on heating, but the β domain is clearly visible on cooling. For higher x values the β⟶γ ($x=0.10$ and 0.125) and then the γ′⟶γ ($x>0.15$) transitions are practically only observed on heating.

This interpretation is in perfect agreement with the Arrhenius plot reported by Krok *et al.*[14] for BIZNVOX.05 where a single conductivity jump is observed on heating between 400 and 500 °C (direct α⟶γ transition), while on cooling the successive γ⟶β and β⟶α transitions are clearly visible, at about 480 and 220 °C, respectively. In the same way, the Arrhenius plot reported by the same authors for BIZNVOX.07[14] can be explained by a direct α⟶γ transition around 500 °C on heating, and a large metastable β domain occurring below 450 °C on cooling, without any visible β⟶α transition. This large metastability of the β domain is easily

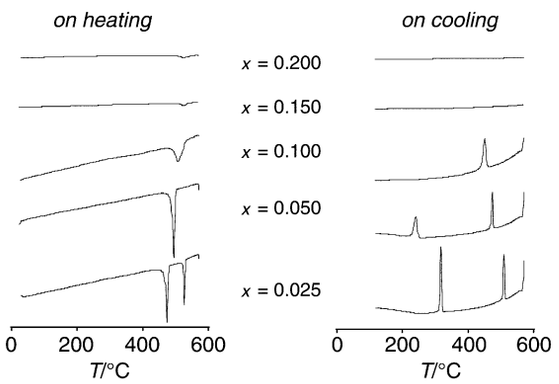

Fig. 8 DSC analyses performed on $Bi_2V_{1-x}Zn_xO_z$.

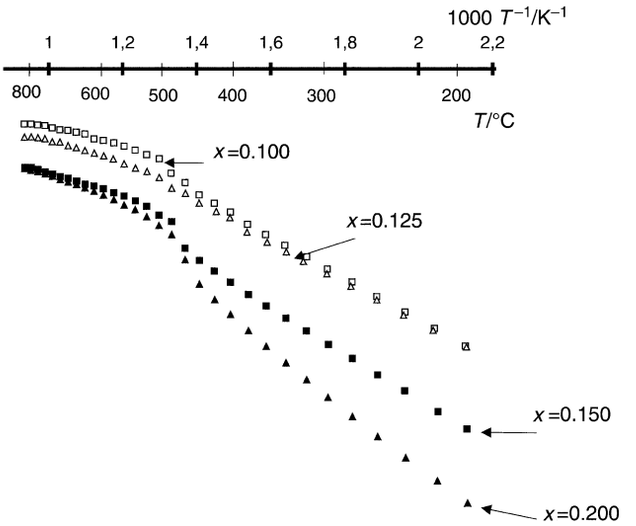

Fig. 9 Arrhenius plots corresponding to $Bi_2V_{1-x}Zn_xO_z$.

explained by the $x=0.07$ value, very close to the critical $x=0.08$ one corresponding to the α⟶β structural change.

The Arrhenius plots of some $Bi_2V_{0.96-x}Zn_xBi_{0.04}O_z$ compounds ($x=0.10$, 0.125 and 0.175) have previously been reported.[13] Those corresponding to $Bi_2V_{1-x}Zn_xO_z$ with $x=0.10$, 0.125, 0.15 and 0.20 are represented on Fig. 9. The conductivity values are practically identical for a given x value, independently of $y=0$ or 0.04, and the maximum σ values are obtained for $x=0.10$ which belongs to the β-type structure. Our σ values are also very similar to those reported by Krok *et al.* for identical compositions.

Usually, for BIMEVOX the best performances are obtained with γ-type solid solutions rather than with β-type ones. But a similar anomaly has already been observed in the BISBVOX family,[18] and this similar γ-like behaviour of BIZNVOX and BISBVOX compounds is likely due to the very small difference between the a_m and b_m parameters of the mean cell in the β-type domain: $a-b\approx0.02$ Å (see Fig. 6).

SAED and HREM studies

The clear and apparently simple one-dimensional incommensurate modulations observed in the α and β domains could lead us to undertake a more detailed structural study based, for example, on X-ray and/or neutron single crystal diffraction data. But prior to this structure determination a selected area electron diffraction (SAED) study was performed to clarify the actual crystallographic symmetry. Different samples corresponding to various Zn contents within the α and β domains were examined and revealed very complex disordered materials. For obvious reasons of clarity the following description will be limited to one composition, chosen as $Bi_2V_{0.875}Zn_{0.125}O_{5.312}$, corresponding to the upper limit of the β-type domain. From the X-ray powder characterization described here above (Fig. 7) the modulation vector (δ) associated to this compound is $0.66a^*$, equivalent to a $3a_m$ superstucture in direct space.

Several electron diffraction patterns (EDP) were collected and, excepting the spots corresponding to the basis mean cell, no supplementary spots nor diffuse streaks were observed along the c direction (the stacking direction of the Bi_2O_2 and perovskite-like sheets of the BIMEVOX structures). This observation is in agreement with the results of similar studies previously performed on $Bi_4V_2O_{11}$,[15] or different BIMEVOX:[12,19,20] all the structural modifications are always observed in the (001) planes in this family.

Some typical EDPs are shown in Fig. 10. Owing to the very close values of the a and b unit cell parameters, the a^* and b^* directions cannot be distinguished. In a general way, the

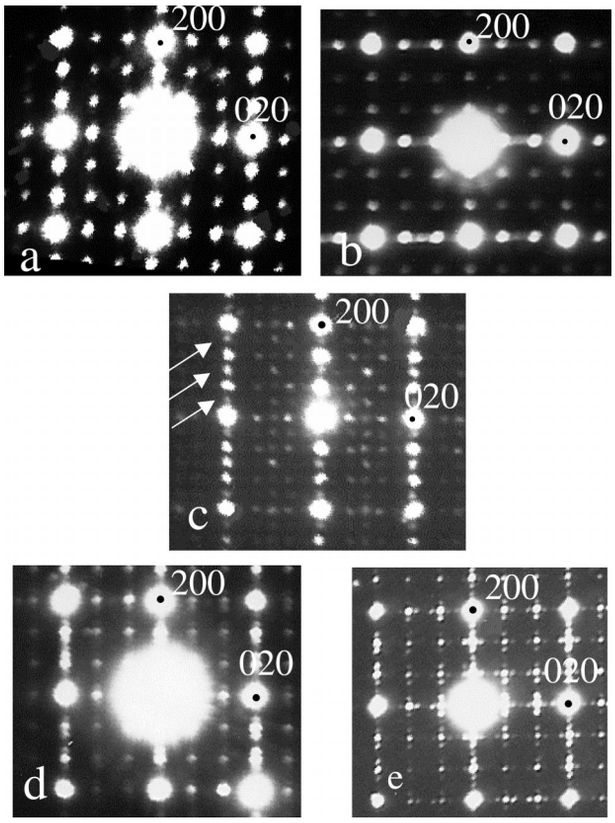

Fig. 10 $Bi_2V_{0.875}Zn_{0.125}O_z$: some typical [001] EDPs. In general a tripling of the mean cell is systematically observed. (a) A two-dimensional modulation is suggested; (b) Such a pattern could result from a twinning with one predominant domain; (c) In addition to the spots associated to the tripling of the parameter(s), supplementary spots (arrows) are seen characterising a higher periodicity; (d) and (e) show even more complex EDPs.

tripling of the mean cell is systematically observed, in accordance with the X-ray powder diffraction study, but much more complex additional modulations are revealed. For instance in Fig. 10a we see additional spots along both axes and away from the axes, having similar intensities, which could suggest a two-dimensional modulation $\boldsymbol{q} \approx 0.66(na^* + mb^*)$ system, similar to that previously observed in BICOVOX.15.[21] The EDP of Fig. 10b is related to another crystal where the satellite spots corresponding to the tripling of the lattice parameter are significantly more intense along one direction than along the perpendicular one. Such a pattern could result from a twinning with one predominant domain. Some additional low intensity spots, away from the axis, could be due to double diffraction. The EDP of Fig. 10c displays, in addition to the spots associated to the tripling of the parameter(s), supplementary spots (arrows) characterising a higher periodicity ($\approx 6a_m$), as observed in α-$Bi_4V_2O_{11}$.[15] The EDP of Figs. 10d and 10e are even more complex: the satellite spots of the basic modulation $\boldsymbol{q} \approx 0.66a_m^*$ (and/or b_m^*) are surrounded by additional spots along one or two perpendicular directions, and even by diffuses streaks.

The EDPs of Figs. 11a and 11b were obtained with a smaller area diffraction aperture and correspond to two different zones of the same crystal. Fig. 11a (zone 1) reveals modulation spots with different intensities along the (200) and (020) directions, which could be due to a twinned zone. The most intense modulation is always $\boldsymbol{q} \approx 0.66a_m^*$ (and/or b_m^*), but a further modulation corresponding to about a four-fold higher periodicity is also visible. The EDP of the second zone (Fig. 11b) exhibits satellite spots with equivalent intensities but with a three-fold periodicity along one direction, and a twelve-fold one along the perpendicular direction.

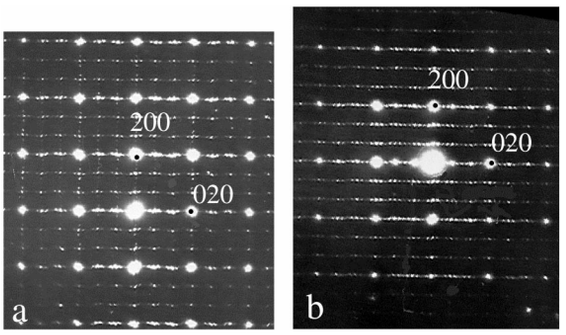

Fig. 11 $Bi_2V_{0.875}Zn_{0.125}O_z$: [001] EDPs corresponding to two different zones of the same crystal. A tripling of the mean cell is systematically observed: (a) likely due to a twinned zone and (b) a further modulation corresponding to about a four-fold higher periodicity is visible.

A high resolution (HREM) study of this crystal was carried out (zones 1 and 2). Owing to the sensitivity of these materials to reduction, detailed in our previous study dealing with the transformation occurring in $Bi_4V_2O_{11}$, when submitted to the focused electron beam leading to $Bi_4V_2O_{10.66}$ or $Bi_4V^{IV}_{1/3}V^{V}_{2/3}O_{10.66}$,[15] a systematic comparison of the EDPs before and after HREM was made. No apparent modification was observed which would express a significant reduction.

To ascertain this observation, an *in situ* reduction of the same BIZNVOX.125 sample was studied by X-ray powder diffraction on a Siemens D5000 diffractometer under a H_2/N_2 flow. The sample was first heated under air up to 350 °C at 0.2 °C s^{-1}. The atmosphere was then purged of oxygen by a nitrogen flow over a period of 45 minutes before introduction of the H_2/N_2 flow (2.5 l h^{-1}/2.5 l h^{-1}). A diagram was recorded every 15 minutes. Due to the low resolution of the PSD detector, it was not possible to resolve *hkl*/*khl* doublets. The different diffractograms collected under this reductive atmosphere are reported in Fig. 12. Unlike the significant modifications observed on $Bi_4V_2O_{11}$[15] under the same operating conditions, the evolution is softer in this case. However, a careful examination of the diffractograms enables us to point out, during the first three hours of the experiment, a small shift of the 020/200 reflections (indexed in the "mean cell") towards higher 2θ values (decreasing *a* and *b* parameters), concomitant with an opposite shift of the 006 reflection towards smaller 2θ values (increasing *c* parameter). Moreover, a progressive but rapid (45 min) disappearance of the $3a_m$ modulation is also to be noticed. This evolution is stabilised after about 4 hours of experiment while two new peaks at $2\theta \approx 51$ and 63° progressively grow up. We have not, as yet, managed to identify these

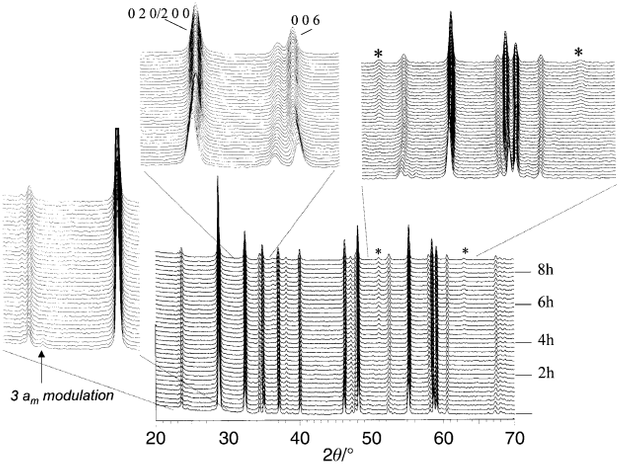

Fig. 12 HTXRD of BIZNVOX.125 performed under a H_2/N_2 reductive atmosphere at 350 °C.

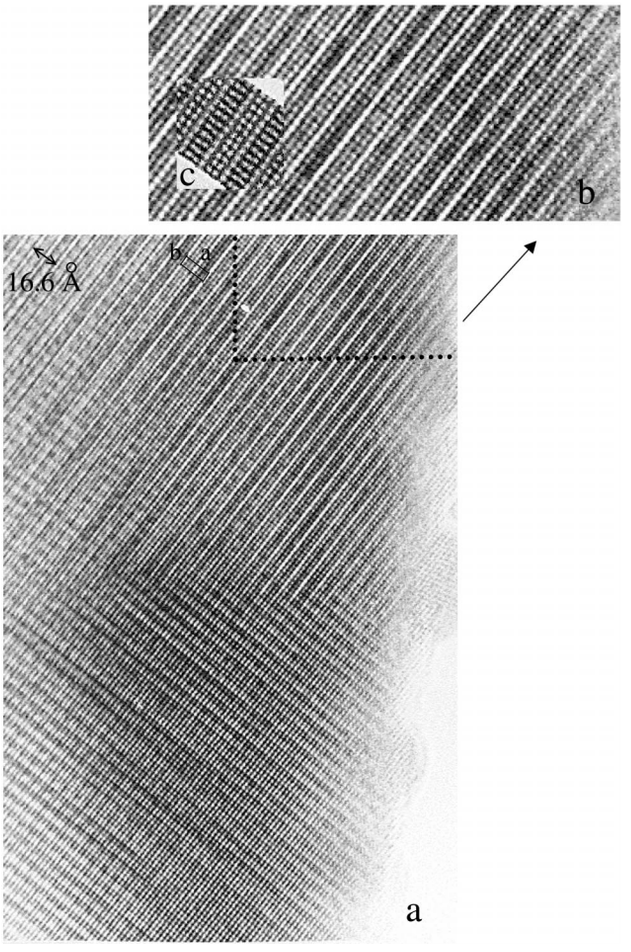

Fig. 13 $Bi_2V_{0.875}Zn_{0.125}O_z$: HREM image corresponding to the EDP of Fig. 11a. (a) Confirms the twinning (90°); (b) Enlargement of a non-twinned zone; (c) A very good agreement occurs between the experimental and calculated image for a defocus of 300 Å and a thickness of 40 Å. The cations appear as bright dots.

peaks, but owing to their low intensity they could correspond to a new modulation characterising this reduced phase. After cooling the sample back to room temperature, no bismuth trace was evidenced. A TGA analysis was performed under a similar reductive atmosphere and revealed a change of the oxygen stoichiometry δ lower than 0.05 for a $Bi_2V_{0.875}Zn_{0.125}O_{5.312-\delta}$ compound. Therefore the BIZNVOX phases appear to be less sensitive to reduction than the undoped parent compound $Bi_4V_2O_{11}$. As the $3a_m$ modulation was recovered after HREM images, we can thereby reasonably expect that no significant damage of the material occurred during the experiment and that the obtained images are representative of the oxidised phase.

Fig. 13 is the image corresponding to the EDP of Fig. 11a (zone 1). This image confirms the twinning (90°), but in the untwinned area (left hand part), we observe regular fringes characterised by dark and bright stripes. As the main modulation in this compound is similar to the main superstructure observed in α-$Bi_4V_2O_{11}$ ($3a_m$), we tried to simulate this image using our atomic coordinates obtained from single crystal X-ray diffraction data collected in a threefold supercell of α-$Bi_4V_2O_{11}$.[22] Several simulations were made, for various defocus and thickness values, and a very good agreement was obtained between the calculated and experimental images for a defocus value of 300 Å and a thickness of 40 Å (Fig. 13b). The only atomic coordinates used in this calculation were those of the Bi^{III} and V^{V} cations. Fig. 14 shows the (001) projection of the cationic positions corresponding to one V slab encaged inbetween two consecutive Bi sheets: a typical coupling between the undulations of the V and the Bi lines is observed, which is sufficient to account for the contrast observed. In the theoretical image the cations appear as bright dots and the intense bright lines correspond to the non-undulated lines [(**1**) in Fig. 14] while the less intense bright dots correspond to the undulated lines [(**2**) in Fig. 14]. Moreover a careful examination of the HREM image (Fig. 13) shows two different contrasts in two consecutive undulated layers which could be interpreted as a small difference in Bi positions between two consecutive undulated Bi sheets. These observations are also in accordance with other experimental results such as X-ray powder diffraction where a relatively high intensity of the satellite peaks is observed; a modulation due only to modification of the O arrangement would not be observable by X-ray diffraction studies.

The HREM image corresponding to the SAED pattern of Fig. 11b is reported on Fig. 15. Keeping in mind the Bravais lattice of the basic mean cell (space group *Fmmm*, $a_m \approx b_m \approx 5.55$ Å), the distance of 2.7 Å between two bright dots, as observed in the thick part of the crystal, corresponds effectively to this periodicity. But another modulation is observed along the perpendicular direction (indicated by a horizontal arrow on Fig. 15), corresponding to a further four-fold super periodicity. This latter modulation appears to result from a relative gliding of the sheets which would be equivalent to a super defect at this scale.

All these observations reveal a large variety and complexity in the modulations occurring in this material. This is a typical and general characteristic of the BIMEVOX family of

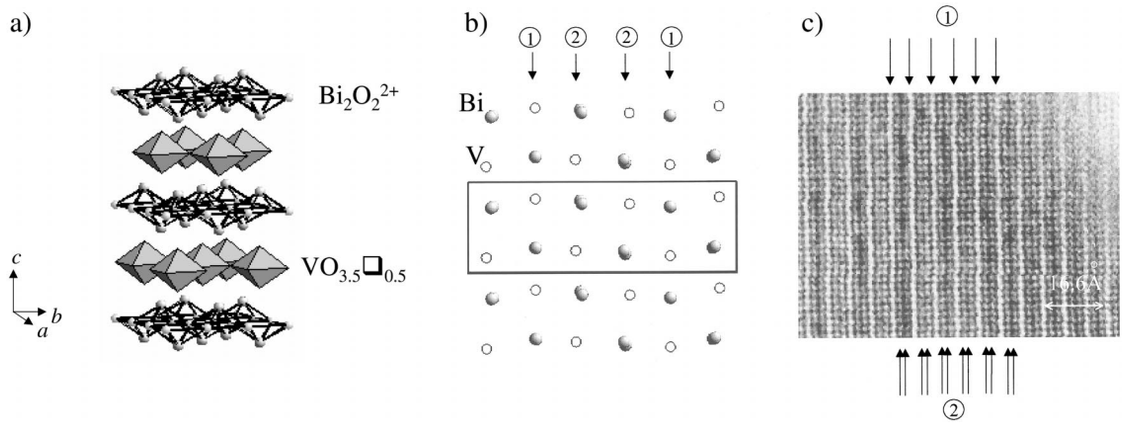

Fig. 14 $Bi_2V_{0.875}Zn_{0.125}O_z$: relationship between the (001) projection of the structure and the (001) HREM image. (a) A schematic representation of the $Bi_4V_2O_{11}$ structure, (b) (001) projection of the structure, (c) (001) HREM image. The intense bright lines correspond to the non-undulated lines (**1**) while the less intense bright dots correspond to the undulated lines (**2**). A typical coupling between the undulations (**2**) of the V and the Bi lines is observed which is sufficient to account for the contrast observed.

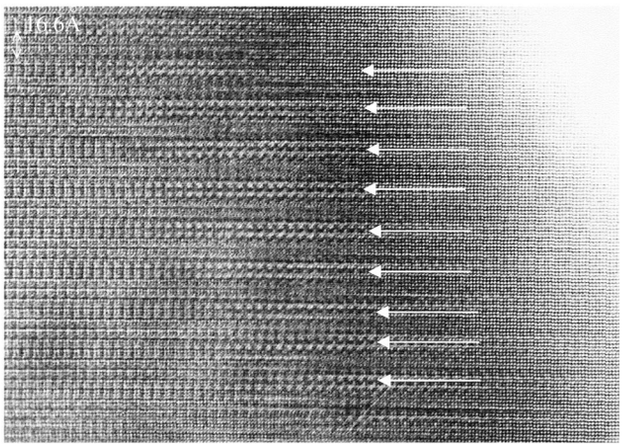

Fig. 15 HREM image corresponding to the SAED pattern of Fig. 11b. Another modulation is observed along the perpendicular direction (indicated by a horizontal arrow), corresponding to a further four-fold super periodicity.

compounds. The fundamental reason for this behavior is likely the lability of the O^{2-} anions within the perovskite-like V–O slabs which generates easy modifications of the V–O polyhedra.

Conclusion

The present studies lead to the following conclusions:

(1) In a general way, the synthesis of $Bi_4V_2O_{11}$ from stoichiometric amount of reagents $2Bi_2O_3$ and V_2O_5 occurs through intermediate formation of both $BiVO_4$ and $Bi_8V_2O_{17}$ which then react which each other to produce $Bi_4V_2O_{11}$.

(2) The limiting loci of the BIZNVOX phases stable at room temperature have been determined in the ternary Bi_2O_3–V_2O_5–ZnO diagram. All phases can be described by the formulation $Bi_2(V_{1-x-y}Zn_xBi_y)O_z$ with maximum x value $=0.25$ when $y=0$ and the maximum y value close to 0.06. α-, β-, and γ-type solid solution domains are revealed depending on the x and y values.

(3) The α- and β-type compounds are incommensurate compositional phases with a lock-in of their wave vectors on the three- and two-fold superstructures of the undoped parent compound $Bi_4V_2O_{11}$, respectively, as revealed by X-ray powder diffraction.

(4) Beyond these basic modulations, SAED patterns show very complex systems of higher order modulations which confirm the high level of disorder in these oxide ion conductors.

Acknowledgements

The authors would like to acknowledge the financial support received from the French and Belgian governments through the TOURNESOL program (01135RH). C.V. and C.P. are also grateful to the CNRS and the Region Nord-Pas de Calais for providing studentships.

References

1 K. R. Kendall, C. Navas, J. K. Thomas and H.-C. zur Löye, *Chem. Mater.*, 1996, **8**, 642.
2 P. Shuk, H.-D. Wiemhöfer, U. Guth, W. Göpel and M. Greenblatt, *Solid State Ionics*, 1996, **89**, 179.
3 N. M. Sammes, G. A. Tompsett, H. Näfe and F. Aldinger, *J. Eur. Ceram. Soc.*, 1999, **19**, 1801.
4 G. Mairesse, *C. R. Acad. Sci. Paris*, 1999, **2**, 651.
5 F. Abraham, M. F. Debreuille-Gresse, G. Mairesse and G. Nowogrocki, *Solid State Ionics*, 1998, **28–30**, 529.
6 G. Mairesse, in *Fast Ion Transport in Solids*, ed. B. Scrosati, A. Magistris, C. M. Mari and G. Mariotto, Kluwer, Dordrecht, 1993, p. 271.
7 O. Joubert, A. Jouanneaux and M. Ganne, *Mater. Res. Bull.*, 1994, **29**, 175.
8 V. Sharma, A. K. Shukla and J. Gopalakrishnan, *Solid State Ionics*, 1992, **58**, 359.
9 A. V. Chadwick, C. Colli, C. Maltese, G. Morrison, I. Abrahams and A. J. Bush, *Solid State Ionics*, 1999, **119**, 79.
10 R. Bacewicz and P. Kurek, *Solid State Ionics*, 2000, **127**, 151.
11 C. K. Lee, G. S. Lim and A. R. West, *J. Mater. Chem.*, 1994, **4**, 1441.
12 S. Lazure, R. N. Vannier, G. Nowogrocki, G. Mairesse, C. Muller, M. Anne and P. Strobel, *J. Mater. Chem.*, 1995, **5**, 1395.
13 S. Lazure, C. Vernochet, RN. Vannier, G. Nowogrocki and G. Mairesse, *Solid State Ionics*, 1996, **90**, 117.
14 F. Krok, I. Abrahams, A. Zadrozna, M. Malys, W. Bogusz, J. A. G. Nelstrop and A. J. Bush, *Solid State Ionics*, 1999, **119**, 139.
15 M. Huvé, R. N. Vannier, G. Nowogrocki, G. Mairesse and G. Van Tendeloo, *J. Mater. Chem.*, 1996, **6**, 1339.
16 R. N. Vannier, G. Mairesse, F. Abraham and G. Nowogrocki, *J. Solid State Chem.*, 1993, **103**, 441.
17 R. N. Vannier, G. Mairesse, F. Abraham and G. Nowogrocki, *Solid State Ionics*, 1995, **80**, 11.
18 O. Joubert, A. Jouanneaux, M. Ganne, R. N. Vannier and G. Mairesse, *Solid State Ionics*, 1994, **73**, 309.
19 O. Joubert, A. Jouanneaux, M. Ganne and M. Tournoux, *Mater. Res. Bull.*, 1992, **27**, 1235.
20 Y. C. Yang, L. Qui, W. T. A. Harrison, R. Christoffersen and A. J. Jacobson, *J. Mater. Chem.*, 1997, **7**, 243.
21 C. Muller, M. Anne and M. Bacmann, *Solid State Ionics*, 1998, **111**, 27.
22 G. Mairesse, unpublished work.